

Effective Theory of Non-Adiabatic Quantum Evolution Based on the Quantum Geometric Tensor

O. Bleu, G. Malpuech, D. D. Solnyshkov

*Institut Pascal, PHOTON-N2, University Clermont Auvergne,
CNRS, 4 avenue Blaise Pascal, 63178 Aubière Cedex, France.*

We study the role of the quantum geometric tensor (QGT) in the evolution of quantum systems. We show that all its components play an important role on the extra phase acquired by a spinor and on the trajectory of an accelerated wavepacket in any realistic finite-duration experiment. While the adiabatic phase is determined by the Berry curvature (the imaginary part of the tensor), the non-adiabaticity is determined by the quantum metric (the real part of the tensor) and allows to determine corrections in the regimes where Landau-Zener approach is inapplicable. The particular case of a planar microcavity in the strong coupling regime allows to extract the QGT components by direct light polarization measurements and to check their effects on the quantum evolution.

PACS numbers:

In 1984, Berry [1] has shown that the quantum evolution in a parameter space leads to the accumulation of an extra phase in the wave function, the famous Berry phase (already known in optics at that time as the Pancharatnam phase [2]). Over the last three decades this concept and its generalization – Berry curvature – were understood to be among the most general in physics. For instance, the concept of topological insulator [3] relies on the Berry phase accumulation over all the states of a complete energy band, which turns out to give an integer topological invariant (the Chern number [4]). Berry curvature also strongly affects the trajectory of an accelerated wave packet creating a lateral drift: an anomalous velocity, transverse to the acceleration. This anomalous velocity is at the origin of many crucial phenomena in physics such as the anomalous Hall effect (AHE) [5–7], the intrinsic Spin Hall effect [8], or the Valley Hall effect [9, 10] in Transition Metal Dichalcogenides (TMDs), the latter being a pillar of the emerging field called “valleytronics” [11].

However, Berry curvature is actually a part of a more general object: the quantum geometric tensor (QGT). The gauge invariant QGT was introduced in 1980 by Provost and Vallery [12] as a part of a geometric approach to quantum mechanics [13]. The imaginary part of this Hermitian tensor corresponds to the Berry curvature [1, 14], whereas its real part defines a Riemannian metric, which allows to measure the distance between quantum states (Fubini-Study metric). Several recent theoretical works discuss the properties of this quantum metric as a way toward adiabatic quantum computation or to the study of phase transitions. [15–17]. In condensed matter, the real part of the QGT has been shown to be linked to the superfluid fraction of flat bands [18, 19], to current noise in an insulator [17], and to Lamb shift analog for exciton states in TMDs [20].

The two parts of the QGT play complementary roles when the Hamiltonian of the system changes over time. The imaginary part (Berry curvature) defines the addi-

tional Berry phase in the adiabatic limit, while the real part (quantum distance) determines the non-adiabaticity (NA), which, in turn, brings a correction to the Berry’s formalism. NA in quantum systems has been studied extensively since the pioneering works of Landau [21, 22], Zener [23], Dykhne [24], and many others [25–27], concerning the regime where the NA is exponentially small, whereas configurations with power-law NA were generally considered as somewhat less interesting [24, 28]. The Landau quasi-classical formalism allows to calculate the final non-adiabatic fraction (transition probability) when the perturbation (coupling between the levels) smoothly vanishes at infinities. However, this approach cannot be applied to a simple yet important situation of a spin following a magnetic field rotating with a constant angular velocity, because the perturbation does not vanish. Berry himself trusted that the NA is exponentially small [1], but that is not the case in the configuration he considered [29], as we shall see below. Moreover, the NA changes during the evolution, and its final value (residual NA) is different from the maximal one. The Landau-Zener formalism allows to find only the former, while the latter is not exponentially small even if the evolution is perfectly smooth. In all these cases, the real part of the QGT allows to quantify the NA and to calculate a correction to the Berry phase.

In this work, we calculate the non-adiabatic corrections (NAC) for the phases and trajectories of wave packets for a finite-time quantum evolution beyond the Landau-Zener approximation. We show that these NACs are quantitatively described by the real part of the QGT, whereas the adiabatic limit is described by the imaginary part (Berry phase). We propose an example of application of this formalism in a specific system: a planar microcavity [30] in the strong coupling regime. We show that the use of such type of photonic structure allows, through simple light polarization measurements, a direct access to the components of the QGT in reciprocal space, providing an answer to an important problem of the re-

cent years – the direct measurement of Berry curvature [31–35]. We consider a practical experimental situation showing how the real and imaginary part of the QGT control the anomalous Hall effect.

Rotation of a spin. The Bloch sphere represents the simplest 2-level system with Berry curvature: a spin, interacting with an applied magnetic field. Any 2-level Hamiltonian can be written as a superposition of Pauli matrices, and thus considered as an effective field acting on a pseudospin.

A spin, which follows a slowly rotating magnetic field, is never perfectly aligned with it, and thus it exhibits fast precession (with frequency Ω) about the magnetic field together with the slow rotation (freq. ω) of both of them in the azimuthal plane (see Fig. 1(a)). This behavior is similar to the rotation of a small wheel attached to a long shaft (Fig. 1(b)): the wheel, rotating around its axis with the angular frequency Ω , at the same time rotates with the frequency ω around the shaft fixation point. For both the spin and the wheel, there is an important rotational energy associated with the large frequency Ω , but another part of the energy is associated with the circular motion ω . Nobody could think of neglecting the kinetic energy of the wheel's motion $mv^2/2$. However, the energy of the spin's slow rotation encoded in the Berry phase has been less evident to see. It can be obtained by applying the energy operator $\hat{E} = i\hbar\partial/\partial t$ to the rotating spinor $\psi(t) = 1/\sqrt{2}(e^{-i\omega t}, 1)^T e^{i\Omega t/2}$ (valid in the limit $\omega \rightarrow 0$), which gives $\langle \hat{E} \rangle = -\hbar\Omega/2 + \hbar\omega/2$.

The first term in this expression is the usual energy of the spin in the magnetic field (the corresponding phase is called "dynamical"), and the second is the energy associated with the Berry phase which naturally appears because of the time dependence of the spinor. For the time $T = 2\pi/\omega$ of one full rotation of the field it gives $\varphi_B = \hbar\omega T/\hbar = \pi$. Taking into account only the interaction of the spin with the magnetic field $-\hbar\Omega\mathbf{S}/2$ is like going into the reference frame of the disk: we should not forget that this frame is moving.

Because of the finite experiment duration, the spin does not perfectly follow the field and gets out of the azimuthal plane, tracing a cycloidal trajectory. The corresponding wavefunction (WF) can be written as

$$\psi(t) = \begin{pmatrix} \cos \frac{\theta(t)}{2} e^{-i\omega t} \\ \sin \frac{\theta(t)}{2} \end{pmatrix} e^{i \frac{\Omega \cos \xi(t)}{2} t} \quad (1)$$

where θ is the polar angle and ξ is the angle between the field and the spin. Averaging this expression over precession time allows obtaining the correction to the energy. The average value of θ for the cycloidal trajectory of Fig. 1(a) corresponds to the equilibrium polar angle $\theta = \pi/2 - \omega/\Omega$, at which the spin can follow the field without precession[29, 36, 37]. Another correction appears from averaging ξ , and the final expression becomes $E = -\hbar\Omega/2 + \hbar\omega/2(1 + 2\omega/\Omega)$, which gives the final extra phase $\varphi = \pi(1 + 2\omega/\Omega)$ or $\Delta\varphi/\varphi_B = 4\pi/(\Omega T)$ for one full rotation time T .

We now calculate the extra phase from the numerical solution of the Schrödinger equation. The total extra phase after one full rotation of the magnetic field is plotted in Fig. 1(c) as a function of the rotation duration T measured in units of precession periods $2\pi/\Omega$, which also corresponds to the frequency ratio Ω/ω or to the number of cycloid arcs. Larger T means slower rotation and the adiabatic limit corresponds to $T \rightarrow \infty$ or $\omega/\Omega \rightarrow 0$. We see that the extra phase indeed converges to the value π predicted by Berry, but the correction is not negligible: $\Delta\varphi/\varphi_B > 30\%$ for $\omega > \Omega/10$. The difference between the exact extra phase and the adiabatical value of π is shown in a Log-Log plot on Fig. 1(d), again as a function of T (black curve). We see that instead of being exponentially small, this correction decreases only as $1/T$. The analytical NAC, $\Delta\varphi/\varphi_B = 4\pi/(\Omega T)$ (red curve), fits the exact result very well [36].

Quantum Geometric Tensor. The QGT allows to generalize the above development to an arbitrary parameter space and to unite both contributions to the extra phase acquired by the wavefunction in a single mathematical entity. It is defined as follows:

$$T_{ij} = \left\langle \frac{\partial}{\partial q_i} \psi \left| \frac{\partial}{\partial q_j} \psi \right\rangle - \left\langle \frac{\partial}{\partial q_i} \psi \left| \psi \right\rangle \left\langle \psi \left| \frac{\partial}{\partial q_j} \psi \right\rangle \right. \quad (2)$$

where ψ is the state WF, q_i and q_j are the coordinates in the parameter space. Initially, the QGT was introduced

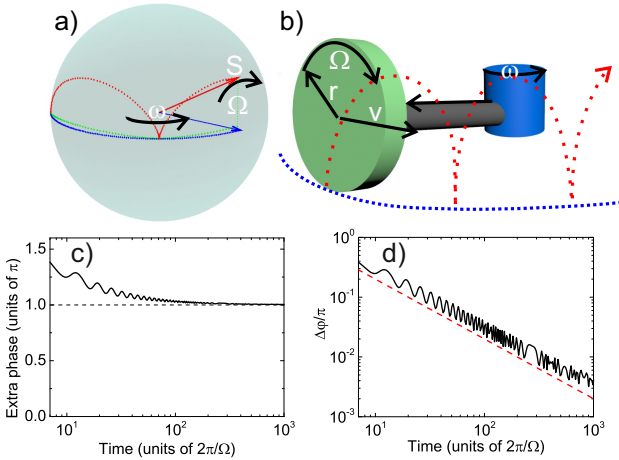


Figure 1: (Color online)(a) Bloch sphere with the spin (red arrow) and the magnetic field Ω (blue arrow), adiabatic trajectory (blue) and real trajectory (red dashed line); (b) Mechanical analog: "adiabatic" trajectory of an infinitely small wheel (blue), cycloid trajectory of a point on a wheel (red). Ω - wheel rotation frequency, v - wheel velocity, ω - shaft center rotation; (c) Total extra phase for one full spinor rotation as a function of the rotation time; (d) Deviation from the adiabatic Berry phase: numerical calculation (black) and analytical correction exhibiting $1/T$ decay (red dashed).

as a phase-invariant quantum metric characterizing the quantum distance between two infinitesimally separated states $ds^2 = 1 - |\langle \Psi(\mathbf{q}) | \Psi(\mathbf{q} + \delta\mathbf{q}) \rangle|^2$ in Hilbert space, also known as Fubini-Study metric:

$$ds^2 = \Re[T_{ij}]dq_idq_j = g_{ij}dq_idq_j \quad (3)$$

Later, it was understood that the imaginary part of this tensor is the Berry curvature:

$$[\mathbf{B}] = 2\Im[T_{ij}] = \Im[\nabla_{\mathbf{q}} \times \langle \Psi(\mathbf{q}) | \nabla_{\mathbf{q}} \Psi(\mathbf{q}) \rangle] \quad (4)$$

which determines the Berry phase for a closed path in the parameter space.

Both components of the QGT contribute to the phase of the WF in any finite-duration experiment: Berry curvature determines the adiabatic value for the phase and the quantum metric (determining the length of adiabatic curve) allows to determine a correction due to the NA, which can be quite important. The average NA fraction (fraction of the excited state in the WF) for a spin on the Bloch sphere can be found as $f_{NA,eq} = \omega^2/4\Omega^2$ [36], which is generalized by using $\omega(q) = 2ds/dt = 2\sqrt{g_{qq}(q)}dq/dt$ and $\Omega = \Omega(q)$:

$$f_{NA,eq}(q) = \frac{g_{qq}}{\Omega^2} \left(\frac{dq}{dt} \right)^2 \quad (5)$$

It determines the corrections to the Berry phase and also to the AHE trajectory for finite-duration experiments in a general parameter space, as we shall see below.

QGT and wavepacket trajectory. Berry curvature has been shown to affect the trajectory of accelerated wavepackets, creating an anomalous velocity contribution in the AHE [5, 6]. The semiclassical equations of motion for the wavepacket center of mass accounting for Berry curvature can be written as [38–40]:

$$\hbar \frac{\partial \mathbf{k}}{\partial t} = \mathbf{F}, \quad \hbar \frac{\partial \mathbf{r}}{\partial t} = \frac{\partial E}{\partial \mathbf{k}} - \hbar \frac{\partial \mathbf{k}}{\partial t} \times \mathbf{B} \quad (6)$$

where, E is the energy dispersion, $\mathbf{B}(k)$ is the Berry curvature and \mathbf{F} is an external force, accelerating the wavepacket. These expressions are derived from a Lagrangian, which includes the total rate of change of the Berry phase over time [6]. Since in finite-time experiments the extra phase includes the NAC (Fig. 1(c,d)), the same correction appears in the Lagrangian and in the equation for the trajectory which reads:

$$\hbar \frac{\partial \mathbf{r}}{\partial t} = \frac{\partial E}{\partial \mathbf{k}} - \hbar \frac{\partial \mathbf{k}}{\partial t} \times 2\Im[\mathbf{T}_{k\phi}] \left(1 + 2 \frac{T_{kk}}{\Omega^2} \left(\frac{\partial \mathbf{k}}{\partial t} \right)^2 \right) \quad (7)$$

This equation is the main result of our manuscript. It shows that the anomalous velocity is a sum of the adiabatic value (as in Eq. (6)) and a NAC (the second term in the parenthesis) which are expressed with QGT components. Below, we consider the specific example of a

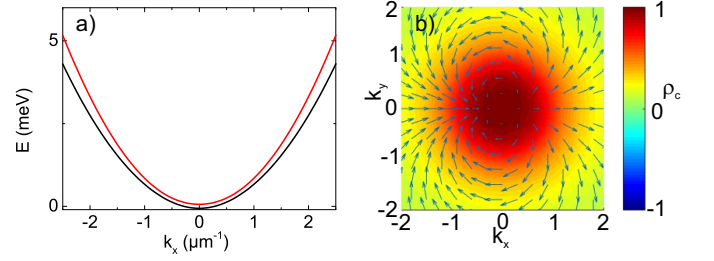


Figure 2: (a) LPB split by Zeeman field and TE-TM SOC; (b) Pseudospin texture of the lower eigenstate: in-plane pseudospin projection (arrows) and S_z (color).

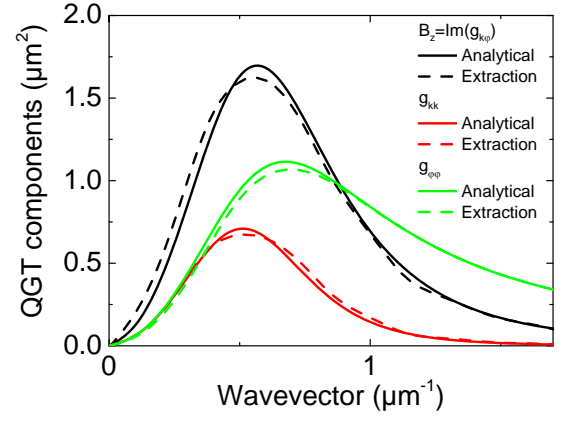


Figure 3: (Color online) QGT components: B_z (black); g_{kk} (red) and $g_{\phi\phi}$ (green) calculated analytically (solid lines) and extracted from numerical experiment (dashed lines).

photonic system, an optical cavity which allows to test this equation and to measure experimentally all quantities, such as the components of the QGT and the real space trajectories.

QGT in a planar cavity. Exploring the whole Bloch sphere requires all 3 components of the effective magnetic field. If one deals with light, it means controlling the splittings between linear polarizations, but also between the circular ones. This is why we have chosen a model system consisting of a microcavity in the strong coupling regime [30], where the polariton modes appear from exciton and photon resonances. The photonic fraction provides a βk^2 in-plane spin-orbit coupling (SOC) due to the TE-TM splitting [41, 42], while the exciton mode provides the Zeeman splitting Δ [43, 44] (under applied magnetic field or thanks to spin-anisotropic interactions [45]). A remarkable feature of this scheme is that the pseudo-spin corresponds to the polarization of light and thus can be easily measured [36].

We begin with the parabolic spinor Hamiltonian of the

lower polariton branch (LPB) of a planar cavity:

$$H = \begin{pmatrix} \frac{\hbar^2 k^2}{2m^*} + \Delta & \beta k^2 e^{2i\phi} \\ \beta k^2 e^{-2i\phi} & \frac{\hbar^2 k^2}{2m^*} - \Delta \end{pmatrix} \quad (8)$$

The eigenvalues of this Hamiltonian are:

$$E_{\pm}(k) = \frac{\hbar^2 k^2}{2m^*} \pm \sqrt{(\Delta^2 + \beta^2 k^4)} \quad (9)$$

These dispersions are shown in Fig. 2(a). We have used $\Delta = 60 \mu\text{eV}$ and $\beta = 0.14 \text{ meV}/\mu\text{m}^{-2}$. While the system clearly shows no gap because of the positive mass of both branches, and therefore is not an example of topological insulator, it nevertheless exhibits a non-zero Berry curvature, created by the pseudospin texture shown in Fig. 2(b). One should note that this dipolar pseudospin texture is also typical for bilayer graphene around K points [46] where quadratic degeneracies can be opened by a bias voltage [47, 48]. The corresponding eigenvectors read:

$$|\Psi_{\pm}(\mathbf{k})\rangle = \begin{pmatrix} \frac{e^{2i\phi}(\Delta \pm \sqrt{\Delta^2 + \beta^2 k^4})}{\sqrt{\beta^2 k^4 + (\Delta \pm \sqrt{\Delta^2 + \beta^2 k^4})^2}} \\ \frac{1}{\sqrt{\beta^2 k^4 + (\Delta \pm \sqrt{\Delta^2 + \beta^2 k^4})^2}} \end{pmatrix} \quad (10)$$

We choose the polar coordinates in the reciprocal space (k, ϕ) to compute analytically the QGT for the lower eigenstate: the metric $g = \Re[T]$ and the Berry curvature $\mathbf{B} = 2\Im[T]$ for the eigenstates aligned with the field.

$$g_{kk} = \frac{\Delta^2 k^2 \beta^2}{(\Delta^2 + \beta^2 k^4)^2}, \quad g_{\phi\phi} = \frac{k^2 \beta^2}{\Delta^2 + \beta^2 k^4} \quad (11)$$

$$g_{k\phi} = g_{\phi k} = 0, \quad \mathbf{B} = \frac{2\Delta k^2 \beta^2}{(\Delta^2 + k^4 \beta^2)^{3/2}} \mathbf{e}_z$$

These are plotted as solid curves in Fig. 3. Because of the k^2 dependence of the TE-TM SOC, the form of the Berry curvature is different from the one of Rashba SOC [7, 39] (with maximum at $k = 0$) and similar to the one of bilayer graphene [49].

A very interesting opportunity to measure these QGT components directly from the polarization of the eigenstates is offered by the radiative states of photonic systems which allows to access all pseudospin components by polarization measurements. The spinor describing arbitrary polarization of light reads: $|\psi\rangle = (\cos\theta/2 e^{-i\varphi}, \sin\theta/2)^T$. The two angles θ and φ can be obtained from the pseudospin as $\theta(k, \phi) = \arccos(S_z)$, $\varphi(k, \phi) = \arctan(S_y/S_x)$. Using that $S_z = S_z(k)$ and $\varphi = \varphi(\phi)$, we derive the analytical formula for

the extraction of the QGT elements from the pseudospin:

$$g_{kk} = \frac{1}{4} \frac{\left(\frac{\partial}{\partial k} S_z(k)\right)^2}{1 - S_z(k)^2} \quad (12)$$

$$g_{\phi\phi} = \frac{1}{4k^2} \left(\frac{\frac{\partial}{\partial \phi} \left(\frac{S_y}{S_x} \right)}{1 + \left(\frac{S_y}{S_x} \right)^2} \right)^2 (1 - S_z^2) \quad (13)$$

$$|\mathbf{B}| = \frac{1}{2k} \left(\frac{\frac{\partial}{\partial \phi} \left(\frac{S_y}{S_x} \right)}{1 + \left(\frac{S_y}{S_x} \right)^2} \right)^2 \frac{\partial S_z}{\partial k} \quad (14)$$

To demonstrate that the QGT components including the Berry curvature can indeed be extracted from a realistic experiment, we perform a numerical simulation using a 2D spinor Schrödinger equation written for LPB in the parabolic approximation:

$$i\hbar \frac{\partial \psi_{\pm}}{\partial t} = -\frac{\hbar^2}{2m} \Delta \psi_{\pm} - \frac{i\hbar}{2\tau} \psi_{\pm} + \Delta \psi_{\pm} + \beta \left(\frac{\partial}{\partial x} \mp i \frac{\partial}{\partial y} \right)^2 \psi_{\mp} + \hat{P} \quad (15)$$

where $\psi_+(\mathbf{r}, t), \psi_-(\mathbf{r}, t)$ are the two circular components, $m = 5 \times 10^{-5} m_{el}$ is the polariton mass, $\tau = 30 \text{ ps}$ the lifetime, \hat{P} is the pump operator which in this case represents uncorrelated noise describing the spontaneous scattering under non-resonant pumping of the exciton reservoir. The results of the extraction are presented in Fig. 3 as dashed curves, whose excellent agreement with the solid lines obtained from the formula (11) confirms the validity of this method.

Figure 4(a) shows the trajectories of polariton wave packet accelerated in a microcavity by a realistic wedge $U(x) = Fx$, where $F = 1 \text{ meV}/128 \mu\text{m}$ for 3 different values of β . The red-dashed curves are analytically calculated using the equation (7) and are in excellent agreement with direct numerical solution of the Schrödinger equation (15) (black curves). The NA fraction can be

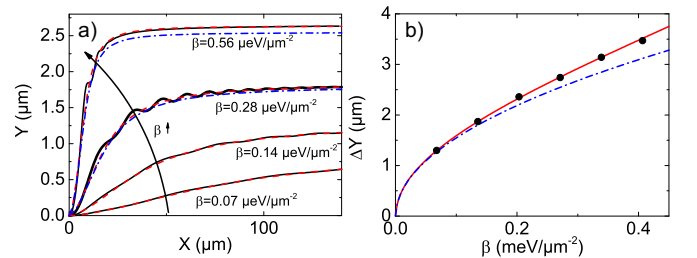


Figure 4: (Color online) (a) Wavepacket trajectories in real space: numerical (black) and analytical (red dashed, uncorrected - blue dash-dotted) for 3 values of TE-TM SOC β ($\Delta = 0.06 \text{ meV}$); (b) Final lateral shift as a function of β : adiabatic (blue dash-dotted line), corrected (red solid line), and numerical (black dots). Here, $\Delta = 0.03 \text{ meV}$.

extracted experimentally by doing polarization measurements: $f_{NA} = S_Y^2$ (see [36] for details). The blue dotted curve shows the trajectory without the correction. Although the difference is small for these parameters, it becomes more important for higher gradients. Fig. 4(b) shows the final lateral shift ΔY as a function of β : adiabatic (blue dotted) and corrected (red) curves, as well as results of simulations (black dots): while the shift follows well the dependence expected from the adiabatic theory $\Delta Y = \sqrt{\beta}\Gamma^2(3/4)/\sqrt{\Delta\pi}$ (see [36]), the numerical results are much better fitted by the theory including the NAC.

To conclude, we have shown that both components of the quantum geometric tensor play an important role for the extra phase in quantum evolution and for the deviation of a wavepacket in any realistic finite-duration experiment: while the adiabatic phase is determined by the Berry curvature (the imaginary part of the tensor), the NAC is determined by the quantum metric (the real part of the tensor). The particular case of a planar microcavity in strong coupling regime allows to extract the QGT components by direct measurements and to check their effects on the quantum evolution.

-
- [1] M. V. Berry, in *Proceedings of the Royal Society of London A: Mathematical, Physical and Engineering Sciences* (The Royal Society, 1984), vol. 392, pp. 45–57.
 - [2] S. Pantharathnam, Proc. Indian Acad. Sci. A **44**, 127 (1956).
 - [3] M. Z. Hasan and C. L. Kane, Rev. Mod. Phys. **82**, 3045 (2010), URL <http://link.aps.org/doi/10.1103/RevModPhys.82.3045>.
 - [4] S. S. Chern, Annals of Mathematics. Second Series **47**, 85 (1946).
 - [5] R. Karplus and J. M. Luttinger, Phys. Rev. **95**, 1154 (1954).
 - [6] G. Sundaram and Q. Niu, Phys. Rev. B **59**, 14915 (1999), URL <http://link.aps.org/doi/10.1103/PhysRevB.59.14915>.
 - [7] N. Nagaosa, J. Sinova, S. Onoda, A. H. MacDonald, and N. P. Ong, Rev. Mod. Phys. **82**, 1539 (2010), URL <http://link.aps.org/doi/10.1103/RevModPhys.82.1539>.
 - [8] J. Sinova, D. Culcer, Q. Niu, N. A. Sinitsyn, T. Jungwirth, and A. H. MacDonald, Phys. Rev. Lett. **92**, 126603 (2004), URL <http://link.aps.org/doi/10.1103/PhysRevLett.92.126603>.
 - [9] D. Xiao, W. Yao, and Q. Niu, Phys. Rev. Lett. **99**, 236809 (2007), URL <http://link.aps.org/doi/10.1103/PhysRevLett.99.236809>.
 - [10] K. F. Mak, K. L. McGill, J. Park, and P. L. McEuen, Science **344**, 1489 (2014).
 - [11] J. R. Schaibley, H. Yu, G. Clark, P. Rivera, J. S. Ross, K. L. Seyler, W. Yao, and X. Xu, Nature Reviews Materials **1**, 16055 (2016).
 - [12] J. Provost and G. Vallee, Communications in Mathematical Physics **76**, 289 (1980).
 - [13] J. Anandan and Y. Aharonov, Phys. Rev. Letters **65**, 1697 (1990).
 - [14] M. Berry, in *Geometric phases in physics* (World Scientific, Singapore, 1989), p. 7.
 - [15] P. Zanardi, P. Giorda, and M. Cozzini, Phys. Rev. Lett. **99**, 100603 (2007), URL <http://link.aps.org/doi/10.1103/PhysRevLett.99.100603>.
 - [16] M. Kolodrubetz, V. Gritsev, and A. Polkovnikov, Phys. Rev. B **88**, 064304 (2013), URL <http://link.aps.org/doi/10.1103/PhysRevB.88.064304>.
 - [17] T. Neupert, C. Chamon, and C. Mudry, Phys. Rev. B **87**, 245103 (2013), URL <http://link.aps.org/doi/10.1103/PhysRevB.87.245103>.
 - [18] S. Peotta and P. Törmä, Nature communications **6**, 8944 (2015).
 - [19] A. Julku, S. Peotta, T. I. Vanhala, D.-H. Kim, and P. Törmä, Phys. Rev. Lett. **117**, 045303 (2016), URL <http://link.aps.org/doi/10.1103/PhysRevLett.117.045303>.
 - [20] A. Srivastava and A. Imamoglu, Phys. Rev. Lett. **115**, 166802 (2015), URL <http://link.aps.org/doi/10.1103/PhysRevLett.115.166802>.
 - [21] L. D. Landau, Phys. Z. Sovjetunion **1**, 88 (1932).
 - [22] L. D. Landau, Phys. Z. Sovjetunion **2**, 46 (1932).
 - [23] C. Zener, Proc. R. Soc. London A **137**, 696 (1932).
 - [24] A. M. Dykhne, Sov. Phys. JETP **11**, 411 (1960).
 - [25] L. D. Landau and E. Teller, Phys. Z. Sowjetunion **10**, 34 (1936).
 - [26] E. C. G. Stueckelberg, Helv. Phys. Acta **5**, 369 (1932).
 - [27] J. P. Davis and P. Pechukas, J. Chem. Phys. **64**, 3129 (1976).
 - [28] L. D. Landau and E. M. Lifshitz, *Quantum Mechanics: Non-relativistic theory* (Pergamon Press, 1991).
 - [29] S. Oh, X. Hu, F. Nori, and S. Kais, Scientific reports **6**, 20824 (2016).
 - [30] A. Kavokin, J. J. Baumberg, G. Malpuech, and F. P. Laussy, *Microcavities* (Oxford University Press, 2011).
 - [31] M. Onoda, S. Murakami, and N. Nagaosa, Phys. Rev. Lett. **93**, 083901 (2004), URL <http://link.aps.org/doi/10.1103/PhysRevLett.93.083901>.
 - [32] G. Jotzu, M. Messer, R. Desbuquois, M. Lebrat, T. Uehlinger, D. Greif, and T. Esslinger, Nature **515**, 237 (2014).
 - [33] T. Ozawa and I. Carusotto, Phys. Rev. Lett. **112**, 133902 (2014), URL <http://link.aps.org/doi/10.1103/PhysRevLett.112.133902>.
 - [34] M. Hafezi, Phys. Rev. Lett. **112**, 210405 (2014), URL <http://link.aps.org/doi/10.1103/PhysRevLett.112.210405>.
 - [35] N. Flaschner, B. S. Rem, M. Tarnowski, D. Vogel, D.-S. Luhmann, K. Sengstock, and C. Weitenberg, Science **352**, 1091 (2016).
 - [36] See Supplemental Material at [URL will be inserted by publisher].
 - [37] H.-A. Engel, E. I. Rashba, and B. I. Halperin, *Theory of Spin Hall Effects in Semiconductors* (John Wiley and Sons, Ltd, 2007), ISBN 9780470022184, URL <http://dx.doi.org/10.1002/9780470022184.hmm508>.
 - [38] D. Culcer, Y. Yao, and Q. Niu, Phys. Rev. B **72**, 085110 (2005), URL <http://link.aps.org/doi/10.1103/PhysRevB.72.085110>.
 - [39] D. Xiao, M.-C. Chang, and Q. Niu, Rev. Mod. Phys. **82**, 1959 (2010), URL <http://link.aps.org/doi/10.1103/RevModPhys.82.1959>.
 - [40] M.-C. Chang and Q. Niu, J. Phys.:Condens. Matter **20**, 193202 (2008).

- [41] G. Panzarini, L. Andreani, A. Armitage, D. Baxter, M. Skolnick, V. Astratov, J. Roberts, A. Kavokin, M. Vladimirova, and M. Kaliteevski, Phys. Rev. B **59**, 5082 (1999).
- [42] A. Kavokin, G. Malpuech, and M. Glazov, Phys. Rev. Lett. **95**, 136601 (2005), URL <http://link.aps.org/doi/10.1103/PhysRevLett.95.136601>.
- [43] J. Tignon, P. Voisin, C. Delalande, M. Voos, R. Houdré, U. Oesterle, and R. P. Stanley, Phys. Rev. Lett. **74**, 3967 (1995), URL <http://link.aps.org/doi/10.1103/PhysRevLett.74.3967>.
- [44] B. Pietka, D. Zygmunt, M. Król, M. R. Molas, A. A. L. Nicolet, F. Morier-Genoud, J. Szczytko, J. Lusakowski, P. Zieba, I. Tralle, et al., Phys. Rev. B **91**, 075309 (2015), URL <http://link.aps.org/doi/10.1103/PhysRevB.91.075309>.
- [45] M. Vladimirova, S. Cronenberger, D. Scalbert, K. V. Kavokin, A. Miard, A. Lemaître, J. Bloch, D. Solnyshkov, G. Malpuech, and A. V. Kavokin, Phys. Rev. B **82**, 075301 (2010), URL <http://link.aps.org/doi/10.1103/PhysRevB.82.075301>.
- [46] A. H. MacDonald, J. Jung, and F. Zhang, Physica Scripta **2012**, 014012 (2012).
- [47] E. McCann, Phys. Rev. B **74**, 161403 (2006), URL <http://link.aps.org/doi/10.1103/PhysRevB.74.161403>.
- [48] E. V. Castro, K. S. Novoselov, S. V. Morozov, N. M. R. Peres, J. M. B. L. dos Santos, J. Nilsson, F. Guinea, A. K. Geim, and A. H. C. Neto, Phys. Rev. Lett. **99**, 216802 (2007), URL <http://link.aps.org/doi/10.1103/PhysRevLett.99.216802>.
- [49] F. Zhang, J. Jung, G. A. Fiete, Q. Niu, and A. H. MacDonald, Phys. Rev. Lett. **106**, 156801 (2011), URL <http://link.aps.org/doi/10.1103/PhysRevLett.106.156801>.
- [50] X. Xu, W. Yao, D. Xiao, and T. F. Heinz, Nature Physics **10**, 343 (2014).

SUPPLEMENTAL MATERIAL

In this supplemental material we discuss the equations on spin dynamics, present the details on the derivation of the non-adiabatic fraction and on its experimental measurements. We also discuss the accelerated wavepacket trajectory with non-adiabatic corrections.

Equations for spin dynamics in a rotating field

We begin with the precession equation for the spin dynamics, which can be obtained from the spinor Schrödinger equation. This equation reads:

$$\frac{d\mathbf{S}}{dt} = \mathbf{\Omega} \times \mathbf{S} \quad (16)$$

Here, $\mathbf{\Omega}(t)$ is the magnetic field vector, which can change both in direction and magnitude in the general case, and \mathbf{S} is the spin vector. To be specific, we consider the rotation of the magnetic field in the equatorial plane.

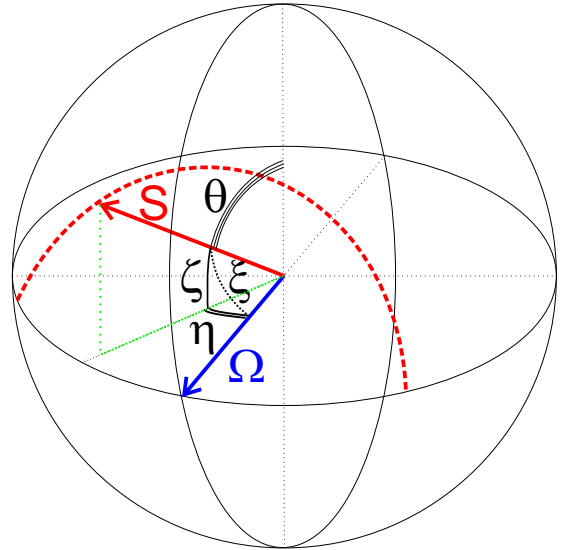


Figure 5: (Color online) The spin vector \mathbf{S} (red), its projection on the equatorial plane (green), and the magnetic field $\mathbf{\Omega}$ (blue) on the Bloch sphere, with the angles used in the supplemental material and in the main text: θ (polar angle of \mathbf{S}), ζ (latitude of \mathbf{S}), η (difference between the longitudes of \mathbf{S} and $\mathbf{\Omega}$), and ξ (angle between \mathbf{S} and $\mathbf{\Omega}$). Red dashed line shows the cycloidal spin trajectory.

The scheme of the Bloch sphere with the spin and the magnetic field and their relative angles is shown in Fig. S5.

Since we are going to study small deviations from the adiabatic regime, the motion of the spin vector is limited to small angles close to the equator of the sphere. We can rewrite the equations using two new variables: the angle between the spin and the equatorial plane ζ (latitude), and the azimuthal angle between the spin projection on this plane and the magnetic field η . These equations read:

$$\begin{aligned} \frac{d\zeta}{dt} &= -\Omega\eta \\ \frac{d\eta}{dt} &= \Omega\left(\zeta - \frac{\omega}{\Omega}\right) \end{aligned} \quad (17)$$

Here, Ω is the magnitude of the magnetic field, while ω is its angular velocity: $\omega = d\phi/dt$ (ϕ is the azimuthal angle of the magnetic field). We see that these equations are similar to the Hamilton's equations for a harmonic oscillator in rescaled coordinates (η plays the role of coordinate q and ζ - the role of momentum p), but with an extra term $d\eta/dt = -\omega$, corresponding to a constant velocity of the harmonic oscillator, meaning that we consider it in a moving reference frame, or that the oscillator itself is moving in our fixed reference frame. This falls very well within the analogy with a rotating wheel considered in the main text.

First of all, we can find a stationary solution:

$$\zeta_{eq} = \frac{\omega}{\Omega} \quad (18)$$

It means that if the magnetic field rotates with a constant angular velocity ω , the spin is able to follow it with the same angular velocity if it is deviated from the equatorial plane towards the pole by ω/Ω . In this case, $\eta = 0$. This solution is very important, because it allows us to estimate the non-adiabaticity in a general case considered below. The fraction of the excited state in the wavefunction is given by:

$$f_{NA} = \left| \left\langle \begin{pmatrix} \cos\left(\frac{1}{2}\left(\frac{\pi}{2} - \theta\right)\right) \\ \sin\left(\frac{1}{2}\left(\frac{\pi}{2} - \theta\right)\right) \end{pmatrix} \middle| \begin{pmatrix} 1/\sqrt{2} \\ -1/\sqrt{2} \end{pmatrix} \right\rangle \right|^2 = \frac{\zeta^2}{4} \quad (19)$$

This fraction is complementary to fidelity $F = |\langle \psi | \psi_0 \rangle|$, where ψ_0 is the ground state in which the system is expected to remain:

$$f_{NA} + F^2 = 1 \quad (20)$$

If at $t = 0$ the spin is not in the position corresponding to the stationary solution (the equilibrium point $\zeta = \zeta_{eq}$, $\eta = 0$), it will precess about the equilibrium position, exactly as the harmonic oscillator with some initial displacement oscillates around the equilibrium point. Since the system of equations is the same as for the harmonic oscillator, its solutions belong to the same family of curves in the phase space (represented here by θ, η): for small angles, these are circular orbits around the equilibrium position, where the radius of the circle is determined by the energy. For example, if at $t = 0$ the spin is in equatorial plane, it will oscillate around the equilibrium position $\zeta_{eq} = \omega/\Omega$, that is, between $\zeta = 0$ and $\zeta = 2\zeta_{eq}$. Its average non-adiabaticity will be given by

$$f_{NA} = \frac{\omega^2}{4\Omega^2} \quad (21)$$

But what if the angular velocity of the rotation of the magnetic field is changing? Changing the ratio ω/Ω corresponds to modification of the equilibrium position of the harmonic oscillator, which is possible under the action of a force. This is not a periodic driving force, contrary to the well-known driven damped oscillator problem, but rather a slowly-varying or stepwise-constant force.

To make this force appear in the equations, let us introduce a new variable $\zeta' = \zeta - \omega/\Omega$. It allows to rewrite the system of equations as follows:

$$\begin{aligned} \frac{d\zeta'}{dt} &= -\Omega\eta - \frac{d}{dt} \frac{\omega}{\Omega} \\ \frac{d\eta}{dt} &= \Omega\zeta' \end{aligned} \quad (22)$$

We see that now the term $d(\omega/\Omega)/dt$ appears in the equation for the momentum derivative, and therefore it indeed plays the role of a force, which determines the equilibrium position. Of course, if a harmonic oscillator is moving (as a whole) and then suddenly stops, or is not moving and then suddenly set into motion, this sudden change excites it and increases the amplitude of its oscillations.

Since the system is not damped, these oscillations cannot decay, and if the angular velocity of the magnetic field is slowly reduced to 0, they will remain and provide a residual non-adiabaticity, which is not exponentially small, but is instead proportional to the derivative $d(\omega/\Omega)/dt$. The fact that if a n -th order derivative of the perturbation experiences a jump, the final transition probability (which is the residual non-adiabaticity in our terms) is not exponential, but proportional to the height of this jump power n , has been obtained in the 30ies within the approach of Landau [28] and is quite well-known, although considered as less interesting than the exponentially small transition probability for a smooth perturbation.

In our case, the residual non-adiabaticity will not play an important role, because it corresponds to oscillations around the equilibrium position. The contribution of these oscillations averages out over time and does not contribute to the wavepacket trajectory (see further sections).

On the other hand, the equilibrium position ζ_{eq} gives a non-vanishing contribution to the final phase and to the wavepacket trajectory via Berry curvature. It is therefore more important in our case to calculate the equilibrium non-adiabaticity as a function of time and to take into account its effects, than to study the residual non-adiabaticity (final transition probability), contrary to the cases considered in the previous works.

Finally, we note that the difference between the exact extra phase (black) and the analytically found solution (red) in Fig. 1d of the main text might be due to the fact that the length of the non-adiabatic cycloidal trajectory is different from the length of the trajectory of the magnetic field [29].

Averaging for the spinor

In the main text, we calculate the average correction to the energy due to the deviation of \mathbf{S} from $\mathbf{\Omega}$. There are two contributions to the energy correction: one from the $\cos\theta/2$ term in the spinor (that is, from the non-zero latitude of the spin), which modifies directly the Berry phase, and one from the magnetic energy term $-\hbar\mathbf{\Omega}\mathbf{S}$, which can also be integrated into a correction for the Berry phase, as we shall see.

The energy operator applied on the spinor gives $\hbar\omega\cos^2\theta(t)/2$, which should be averaged over one precession period $2\pi/\Omega$. The time dependence of $\theta(t)$ is found

from the equations for the spin dynamics: it is simply a harmonic oscillation.

$$\theta(t) = \frac{\pi}{2} - \frac{1 - \cos \Omega t}{2} \frac{\omega}{\Omega} \quad (23)$$

The averaged contribution to the energy reads:

$$\frac{\hbar\omega}{2\pi/\Omega} \int_0^{2\pi/\Omega} \cos^2 \left(\frac{\pi}{2} - \frac{1 - \cos \Omega t}{2} \frac{\omega}{\Omega} \right) dt = \frac{\hbar\omega}{2} \left(1 + \frac{\omega}{\Omega} \right) \quad (24)$$

This is the Berry phase plus a part of the non-adiabatic correction.

The magnetic energy also has to be averaged over time. The angle $\xi(t)$ between \mathbf{S} and $\mathbf{\Omega}$ is given by

$$\xi(t) = \frac{\omega}{\Omega} \sqrt{(1 + \cos \Omega t)^2 + \sin^2 \Omega t} \quad (25)$$

The corresponding contribution to the energy reads

$$-\frac{\hbar\Omega}{2} \cos \xi \approx -\frac{\hbar\Omega}{2} \left(1 - \frac{\xi^2}{2} \right) \quad (26)$$

The averaging gives:

$$-\frac{\hbar\Omega}{2} \left(1 - \frac{1}{2} \frac{\omega^2}{\Omega^2} \frac{1}{2\pi/\Omega} \int_0^{2\pi/\Omega} \left((1 + \cos \Omega t)^2 + \sin^2 \Omega t \right) dt \right) = -\frac{\hbar\Omega}{2} + \frac{\hbar\omega}{2} \frac{\omega}{\Omega} \quad (27)$$

Finally, the energy can be written as:

$$\bar{E} = -\frac{\hbar\Omega}{2} + \frac{\hbar\omega}{2} \left(1 + 2 \frac{\omega}{\Omega} \right) \quad (28)$$

which brings together both non-adiabatic corrections to the Berry phase. While both are important for Fig. 1c,d of the main text, only the spinor part plays a role for the wavepacket trajectory (Fig. 4 of the main text), since the latter is determined by the Berry curvature, as we will show below.

Correction for the Berry curvature

The semi-classical equations for the wavepacket dynamics [6] contain the Berry curvature terms which can be written in tensor form as:

$$B_{i,j} = i \left(\left\langle \frac{\partial \psi}{\partial q_i} \middle| \frac{\partial \psi}{\partial q_j} \right\rangle - \left\langle \frac{\partial \psi}{\partial q_j} \middle| \frac{\partial \psi}{\partial q_i} \right\rangle \right) \quad (29)$$

Only the imaginary part of this expression should be taken. For the spin on the Bloch sphere, the derivatives are taken with respect to θ and ϕ , and the latter derivative is accompanied with $1/\sin \theta$ in spherical coordinates. To simplify the calculation of the correction to the Berry phase regardless of the direction of the rotation of the magnetic field, one needs to write the spinor in the proper gauge, where the Berry connection for θ is nonzero:

$$|\psi\rangle = \frac{1}{2} \begin{pmatrix} (e^{i\theta} + 1) e^{-i\varphi} \\ -i(e^{i\theta} - 1) \end{pmatrix} \quad (30)$$

We need to calculate the non-adiabatic correction to both terms in the expression for Berry curvature. Each derivative corresponds to the rotation of the magnetic field along the corresponding direction (in the equatorial plane for φ and towards the pole for θ), and the non-adiabatic correction appears because of the deviation of the spin from the field: we have to replace θ by $\theta - \zeta_{eq}$ and φ by $\varphi + \varphi_{eq}$ (because increasing θ means going towards the south pole), where both ζ_{eq} and φ_{eq} are equal to the equilibrium deviation angle ω/Ω . The first term in the Berry curvature then reads:

$$\frac{1}{4} \left\langle \frac{\partial}{\partial \theta} \begin{pmatrix} (e^{i\theta} + 1) e^{-i(\varphi + \varphi_{eq})} \\ -i(e^{i\theta} - 1) \end{pmatrix} \middle| \frac{1}{\sin(\theta - \zeta_{eq})} \frac{\partial}{\partial \varphi} \begin{pmatrix} (e^{i(\theta - \zeta_{eq})} + 1) e^{-i\varphi} \\ -i(e^{i(\theta - \zeta_{eq})} - 1) \end{pmatrix} \right\rangle = -\frac{1}{4} \left(1 + i \frac{\omega}{\Omega} \right) \left(\frac{1 - i \frac{\omega}{\Omega} + e^{-i\theta}}{\sin(\theta - \zeta_{eq})} \right) \quad (31)$$

The second term is the complex conjugate of the first one. Subtracting it and keeping only imaginary part of the resulting expression, one obtains the Berry curvature (including non-adiabatic correction):

$$B_{\theta\varphi} = -\frac{1}{2} \frac{\sin \theta}{\sin(\theta - \zeta_{eq})} \quad (32)$$

The real part gives a correction to the metric that we neglect.

If we consider the evolution along a geodesic line on a sphere (to which our previous calculation of ζ_{eq} actually applies), which is a great circle, we can always choose the coordinates in such a way that this great circle is the equator of the sphere ($\theta = \pi/2$). In this case, the

corrected Berry curvature reads:

$$B_{\theta\varphi} = -\frac{1}{2\cos(\zeta_{eq})} \approx -\frac{1}{2\left(1 - \frac{\omega^2}{2\Omega^2}\right)} = -\frac{1}{2}\left(1 + \frac{\omega^2}{2\Omega^2}\right) \quad (33)$$

Using the previously calculated fraction of the excited state $f_{NA} = \omega^2/4\Omega^2$, we can rewrite the corrected Berry curvature as

$$B_{\theta\varphi} \approx -\frac{1}{2}(1 + 2f_{NA}) \quad (34)$$

This correction to the Berry curvature rewritten using QGT appears in Eq. (7) of the main text and allows to calculate the wavepacket trajectory. Putting it short, the first-order correction obtained in the first section cancels out for Berry curvature, but a second-order correction arises from the $1/\sin\theta$ coefficient of the derivative over azimuthal angle φ .

General non-adiabatic evolution

Now we can apply the new equations to determine the non-adiabaticity of a polariton wavepacket, accelerated in combined TE-TM and Zeeman fields. In this case the total magnetic field reads:

$$\Omega = \sqrt{\Delta^2 + (\beta k^2)^2} \quad (35)$$

When the polaritons propagate in a constant gradient, their wave vector increases linearly with time: $k = Ft/\hbar$, where the force can be obtained for example by applying a gradient $F = -\nabla U$. The angular velocity of the rotation of the total magnetic field can be obtained as:

$$\omega = \frac{d\varphi}{dt} = \frac{2ds}{dt} = 2\frac{ds}{dk}\frac{dk}{dt} = \frac{2F}{\hbar}\sqrt{g_{kk}} \quad (36)$$

which gives

$$\omega = \frac{2F}{\hbar} \frac{\Delta\beta k}{\left(\Delta^2 + (\beta k^2)^2\right)}$$

The wavepacket is created at $k = 0$ and accelerated towards $k = \infty$. Its non-adiabaticity can be obtained as

$$f_{NA}(k) = \frac{1}{4} \min(\theta_{eq}^2, \theta_0^2) \quad (37)$$

where

$$\theta_{eq}^2 = \left(\frac{2F}{\hbar}\right)^2 \frac{\Delta^2\beta^2 k^2}{\left(\Delta^2 + (\beta k^2)^2\right)^3} \quad (38)$$

and

$$\theta_0^2 = \frac{\beta^2 F^2}{\Delta^6 \hbar^2} \quad (39)$$

The latter gives us the residual non-adiabaticity measured at large wavevectors and times. We see that it is not exponential in F , but linear, because the configuration of the experiment is different from that of Landau-Zener: instead of slowly increasing the perturbation with time (when we approach the "coupling region" from $-\infty$), we suddenly turn it on at $t = 0$.

Since the residual non-adiabaticity corresponds to precession around $\theta_{eq} = 0$, it does not contribute to the extra phase or to the wavepacket trajectory, and does not appear in the dynamical equations in the main text. For realistic parameters of microcavities, the residual non-adiabaticity looks to be inaccessible, requiring long propagation distances. Therefore, the expression for the non-adiabaticity is simplified, and one can write it as:

$$f_{NA}(k) = \frac{F^2 g_{kk}}{\hbar^2 \Omega^2} \quad (40)$$

We stress that the non-adiabatic fraction and the corresponding correction are calculated from the adiabatic metric.

Experimental measurement of non-adiabaticity

In the precise configuration we consider, the non-adiabaticity of the wavepacket can be measured via the diagonal polarization degree. For this, one should orient the cavity in such a way that the wedge points in the X direction. Then, the "horizontal" polarization should be chosen parallel to this X axis. In this case, the adiabatic evolution means that the spin rotates from the Z axis (circular eigenstate at $k = 0$) to the X pseudospin axis (horizontal polarization), while the deviation from this rotation is necessarily towards the Y pseudospin axis (diagonal polarization).

The three pseudospin components can be extracted from the spatially-integrated intensities measured in 3 pairs of orthogonal polarizations:

$$S_x = \frac{I_H - I_V}{I_H + I_V}, \quad S_y = \frac{I_D - I_A}{I_D + I_A}, \quad S_z = \frac{I_+ - I_-}{I_+ + I_-} \quad (41)$$

Figure 1 shows the agreement between the nonadiabaticity, given by the S_Y^2 pseudospin component, calculated by solving full Schrodinger equations (black), the simple spin dynamics equation, Eq. (17) (blue), and given by the component of the QGT, Eq. (40) (red dashed). We see that the latter captures very well the behavior of the full system, and that the spin dynamics equation for small angles is sufficiently precise. The figure is plotted for $\beta = 0.14 \text{ meV}/\mu\text{m}^{-2}$. The inset shows

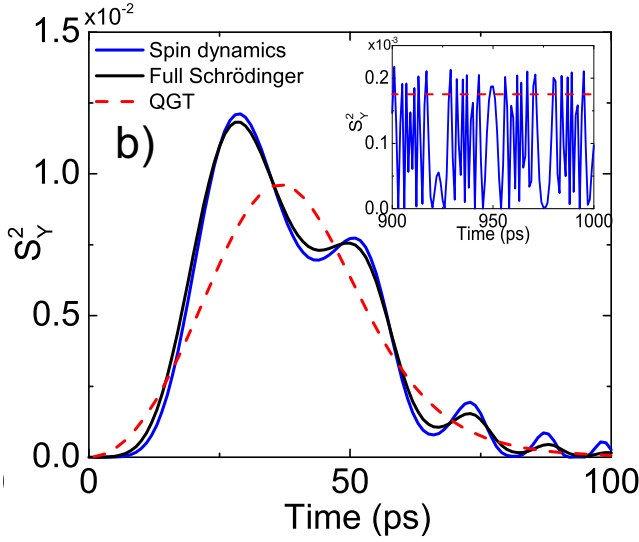


Figure 6: (Color online) The nonadiabaticity (S_Y^2), calculated using the full Schrodinger equation (black), the spin dynamics equation (red), and the QGT (blue dashed).

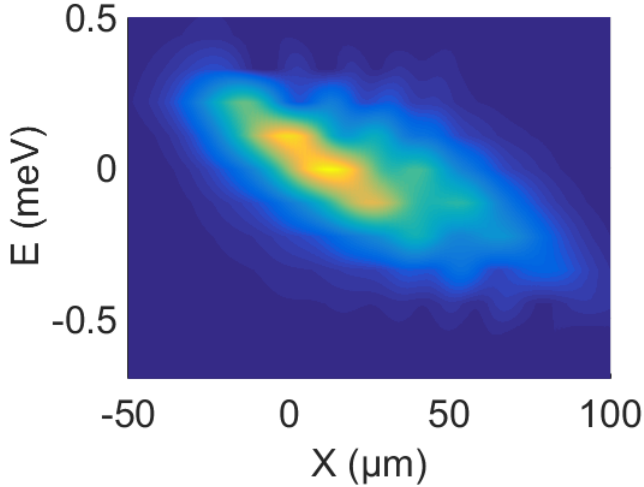


Figure 7: (Color online) Energy-resolved spatial image of emitted intensity $|\psi(x, E)|^2$ for a time window.

the residual non-adiabatic fraction $f_{NA,0}$ (blue) and the analytical value given by Eq. (39) (red dashed).

Another option to measure the non-adiabaticity could be to analyze the spectrum of the wavefunction, because the energy of the ground and excited states is different. However, this approach encounters difficulties in the experimental setting that we propose because of the spatial gradient which accelerates particles. Indeed, different points of the wavepacket have different potential energy at a given moment of time. Moreover, since the wavepacket propagates down the slope, its energy changes quite rapidly over time. Still, it is possible to use a time window and see the excited state in the energetically and spatially resolved emission intensity $|\psi(x, E)|^2$, as shown in Fig. S7.

Wavepacket trajectory

The anomalous Hall effect with Rashba-type SOC (linear in k) is quite well-known, and the corresponding Berry curvature and trajectory (without non-adiabatic corrections) have been calculated before. This configuration corresponds both to Dirac Hamiltonian describing an electron in vacuum [40] and to electrons in 2D materials (like Transitional Metal Dichalcogenides), which obey to an effective Dirac Hamiltonian [50].

At the same time, the case of k^2 TE-TM SOC with double winding has not been studied, although it is quite important for photonics. In this section, we present the detailed results concerning the trajectory of an accelerated wavepacket (under the effect of a force F) in presence of the TE-TM SOC and a constant magnetic field providing Zeeman splitting, solving equations (6) and (7) of the main text.

The analytical solution of eq. (6) which does not include the non-adiabatic correction reads:

$$x(t) = \frac{Ft^2}{2m} - \frac{\sqrt{\Delta^2 + \frac{\beta^2 F^4 t^4}{\hbar^4}}}{F} + \frac{\Delta}{F} \quad (42)$$

and

$$y(t) = \frac{F^3 \hbar t^3 \beta^2 \sqrt{\Delta^2 + F^4 t^4 \beta^2 / \hbar^4} \left(3 - \left(1 + \frac{F^4 t^4 \beta^2}{\Delta^2 \hbar^4} \right) {}_2F_1 \left(1, \frac{5}{4}, \frac{7}{4}, -\frac{F^4 t^4 \beta^2}{\Delta^2 \hbar^4} \right) \right)}{3(\Delta^3 \hbar^4 + \Delta F^4 t^4 \beta^2)} \quad (43)$$

The maximal shift of the wavepacket in the Y direction at $t \rightarrow \infty$ is given by:

$$y_\infty = \frac{\sqrt{\beta} \Gamma^2 \left(\frac{3}{4} \right)}{\sqrt{\Delta} \sqrt{\pi}} \quad (44)$$

We see that increasing the lateral shift requires increasing the TE-TM splitting β or decreasing the magnetic field Δ .

The importance non-adiabatic correction can be esti-

mated by the maximal value of the non-adiabatic fraction f_{NA} behaves as:

$$f_{NA,max} \propto \frac{\beta}{\Delta^3} \quad (45)$$

To reduce the maximal non-adiabaticity, it is therefore important to have a sufficiently large Zeeman splitting Δ .

To have a maximal displacement and a good adiabaticity at the same time, it is better to increase the TE-TM SOC β instead of reducing the magnetic field Δ , because the non-adiabaticity behaves as $1/\Delta^3$.

The analytical solution for the equation (7) of the main text including the non-adiabatic correction can also be found:

$$y(t) = \frac{F^3 \beta^3 \left(\Delta t \left(15 + 2\Delta^2 \left(70t^2 + \frac{-15\Delta^4 \hbar^{12} + 8\Delta^2 F^4 \hbar^8 t^4 \beta^2 + 3F^8 \hbar^4 t^8 \beta^4}{(\Delta^2 \hbar^4 + F^4 t^4 \beta^2)^3} \right) \right) + \frac{5(-1)^{3/4} \Delta \hbar \sqrt{\frac{\Delta}{\beta} + \frac{F^4 t^4 \beta}{\Delta \hbar^4}} \nu}{F^3 \beta} \right)}{140\Delta^4 \hbar^3 \sqrt{\Delta^2 + F^4 t^4 \beta^2 / \hbar^4}} \quad (46)$$

where

$$\nu = 28\Delta^3 \hbar^2 E \left(i \operatorname{arcsinh} \left(\frac{Ft \sqrt{\frac{i\beta}{\Delta}}}{\hbar} \right), -1 \right) + (-28\Delta^3 \hbar^2 + 3iF^2 \beta) F \left(i \operatorname{arcsinh} \left(\frac{Ft \sqrt{\frac{i\beta}{\Delta}}}{\hbar} \right), -1 \right) \quad (47)$$

where E and F are the elliptic integrals of the second kind. Unfortunately, we did not manage to find the limit of this expression for $t \rightarrow \infty$.

From the practical point of view, the above analytical expressions for $y(t)$ appear quite cumbersome, and we

advise the direct numerical solution of equations (6) and (7), because the calculation time of the hypergeometric function and the elliptic integrals is quite comparable or even longer than the direct solution of the equations, while the results are identical.